THE ASTROPHYSICAL JOURNAL, 276:560–571, 1984 January 15

A HIGH-RESOLUTION STUDY OF HERBIG-HARO OBJECTS 1 AND 2[1]

L. HARTMANN AND J. C. RAYMOND
Harvard-Smithsonian Center for Astrophysics
Received 1983 February 22; accepted 1983 June 23

ABSTRACT

We have observed Herbig-Haro objects 1 and 2 with high spectral and spatial resolution in order to test shock models for the line emission. A detailed bow shock model has been constructed which yields line widths and optical and UV spectra in reasonable agreement with observation for maximum shock velocities ~ 200 km s^{-1}. Such velocities are comparable to the transverse velocities of the knots in HH 1 and 2 inferred from proper motion studies.

The observations suggest that HH objects are rapidly moving, dense clouds shocking with less dense interstellar medium. The large energy requirements of these objects, combined with their small apparent size as seen from the exciting star, seem to require unreasonably large stellar mass loss rates. However, it is possible that the HH objects subtended a much larger solid angle at the star when originally accelerated.

Subject headings: interstellar: matter — nebulae: general — shock waves — stars: mass loss — stars: pre-main-sequence

I. INTRODUCTION

The line emission from Herbig-Haro (HH) objects has been attributed to the passage of shock waves through dense material in regions of star formation (Schwartz 1975, 1978; Dopita 1978; Raymond 1979). Although the shock model has been relatively succesful in explaining many features of the observations, a number of problems still remain. One difficulty is the indication of different shock velocities from different line ratios. For example, ultraviolet observations of HH 1 indicate shock velocities ~ 200 km s^{-1} are required to produce the high-temperature emission observed (Böhm, Böhm-Vitense, and Brugel 1981), while the O III/Hβ ratios generally suggest much lower shock velocities (Dopita 1978; Raymond 1979). There is some uncertainty in the amount of extinction in these regions, which affects the derived power emitted in the ultraviolet spectrum considerably. Recent discussions of the UV continuum have centered on whether it can be produced by two-photon emission (Böhm, Böhm-Vitense, and Brugel 1981; Brugel, Shull, and Seab 1982; Dopita, Binette, and Schwartz 1982).

These details are of particular interest because the shocks are thought to be driven by winds from pre-main-sequence stars (cf. Schwartz 1975; Schwartz and Dopita 1980) and so potentially may be used as diagnostics of youthful stellar activity. A variety of models have been developed to explain the energetics of HH objects (cf. Schwartz 1975; Schwartz and Dopita 1980; Cantó 1980; Cantó and Rodríguez 1980; Norman and Silk 1979; Königl 1982), but observational studies have not clearly established a preference for any particular theory, and it has proved difficult to understand the observed emission in the context of typical pre-main-sequence winds (Mundt and Hartmann 1983). Our interest is to estimate the velocity and energy of the ejected material more precisely in order to shed further light on the cause of the observed activity.

In this paper we present observations of the HH 1 and HH 2 emission knots with the high spectral and spatial resolution essential to properly interpret these complicated objects. A bow shock model has been developed which reproduces many of the detailed features of the observations. The principal conclusion of the comparison between observation and theory is that the shock velocities necessary to account for both the excitation and line widths are substantially larger than previously thought. The shock velocities are comparable to the transverse velocities of the knots in HH 1 and HH 2 measured by Herbig and Jones (1981). We also find weak correlations in the data which suggest that shock velocities increase with increasing proper motion. The simplest explanation of these results is that the HH objects are dense clouds which are colliding with less dense, stationary interstellar gas, though this interpretation is not entirely free of difficulties. Finally, we consider the implications of our observations concerning the source of HH object activity.

II. OBSERVATIONS

The data reported here were acquired during three observing runs in 1981 November and December and 1982 November at the Multiple Mirror Telescope Observatory on Mount Hopkins. The detector was a photon-counting intensified Reticon (Latham 1982). One series of observations was made with the Agassiz echelle spectrograph, using a projected slit width of 1.″2 and a length 2.″5 on the sky to study the echelle order centered on Hα (6525 Å $\lesssim \lambda \lesssim$ 6595 Å) with a resolution of about 14 km s^{-1}. Low spectral resolution (~ 10 Å) observations of HH 1 and HH 2 were also made with the MMT spectrograph using a 2″ circular aperture, which permitted analysis of the wavelength region between 3800 Å and 6800 Å.

Wavelength assignments for the high-resolution spectra were derived from a Th-Ar hollow cathode lamp. An incandescent light source was used to remove "fixed-pattern" noise. Unfortunately, during the 1981 November echelle observations electronic problems caused a large and variable

[1] The research reported herein is based upon data acquired at the Multiple Mirror Telescope Observatory (MMTO). The MMTO is a joint facility of the University of Arizona and the Smithsonian Institution.

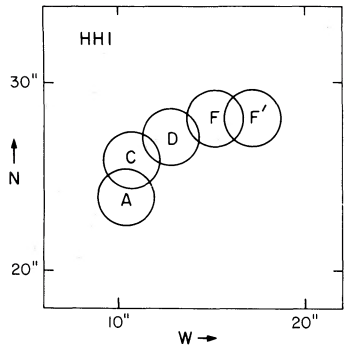

FIG. 1a

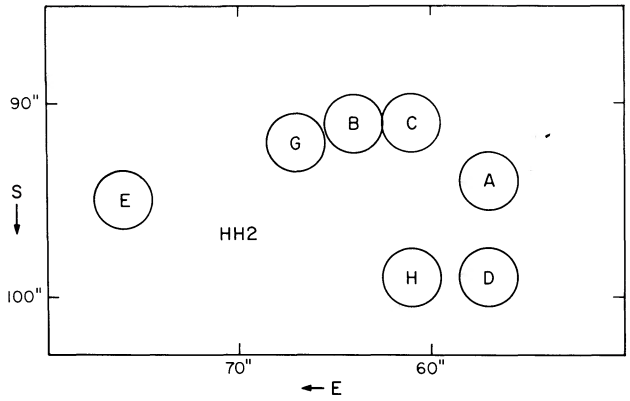

FIG. 1b

FIG. 1.—Positions observed in HH 1 and HH 2, measured relative to the Cohen-Schwartz (CS) star. The 3″ diameter circles indicate upper limits to the areas observed in spectra of individual knots. (*a*) Positions observed in HH 1. (*b*) Positions observed in HH 2.

(quasi-sinusoidal) modulation in the count rates with a period ~ 15 km s^{-1}. The echelle data obtained in 1982 November did not suffer the same difficulties. The echelle blaze response was removed through normalization to the incandescent source.

The fluxes from the MMT spectrograph were placed on a relative scale by observing standard stars. Although this spectrophotometry is not extremely accurate, the relative calibration is probably good to $\lesssim 20\%$, as indicated by comparison with results from Brugel, Böhm, and Mannery (1981) for a few individual knots.

Spectra were taken of knots in HH 1 and HH 2 using the positions given by Herbig and Jones (1981), using offsets from the Cohen-Schwartz (1979) (CS) star. The positions observed are schematically indicated in Figure 1. Considering the slit or aperture used, the seeing, and the tendency of the individual mirrors to drift apart on the sky over exposures longer than 10 minutes, we estimate that the spectra presented here encompass areas $\sim 2''$–$3''$ on the sky.

a) Echelle Observations

In Figure 2 we exhibit Hα profiles of knots in HH 1 and HH 2. Table 1 lists line widths and radial velocities for all of the knots. The structure on small spatial scales is clearly apparent in these data. The HH 1C position is only $\sim 2''$ from the HH 1A knot, and yet the line widths differ by a factor of 2. Even though widths are relatively similar between HH 1C and HH 1F, also separated by $\sim 2''$, the line asymmetry changes significantly. The knots of HH 2 also provide evidence for a complicated flow pattern. In particular, the line profiles of HH 2A′ show extreme asymmetry, with a total velocity width of 300 km s^{-1}. This peculiar shape may reflect the fact that this knot has only recently appeared (Herbig and Jones 1981).

The Hα emission typically exhibits a FWHM ~ 70 km s^{-1}, with a few knots of low excitation like HH 1A and HH 2E (see below) having much narrower widths (FWHM ~ 35 km s^{-1}). Emission from the brightest knots may be traced out to nearly ± 100 km s^{-1} from line center. The [N II] lines have shapes similar to the Hα lines, but they are slightly narrower (cf. Fig. 3). Our results agree reasonably well with Schwartz's (1981) echelle observations of HH 1, assuming that the brightest knots observed here dominate the overall emission.

In Figure 4 we have plotted the FWHM of the Hα emission as a function of radial velocities given by the emission centroids. The range of radial velocities exhibited by HH 2 is much greater than HH 1, as might be expected since HH 2 is much more widely dispersed on the sky. Most of the HH object knots appear to be moving toward us relative to the ^{12}CO cloud emission (Loren, Evans, and Knapp 1979). The radial velocity of the CS star is not well determined; Mundt and Hartmann (1983) estimated $V_R = 15 \pm 5$ km s^{-1}. We suggest that the small blueshift of the HH object knots relative to the C-S star and the surrounding molecular cloud results from the effects of extinction, which favor the detection of knots on the side of the embedding material toward the Earth.

The radial velocities of the knots are much smaller than the transverse velocities ~ 200–300 km s^{-1} inferred from proper motion studies (Herbig and Jones 1981). This implies that most of the motion is directed transverse to the line of sight. The large line widths observed in this study strongly

TABLE 1

Hα AND [N II] VELOCITY CENTROIDS AND WIDTHS

Object	v^a (Hα)	v ([N II])	FWHM (Hα)	FWHM ([N II])
1A (I)[b]	14.7	8.1	43	32
	10.7	7.1	46	51
1C (I)	5.8	−1.5	76	68
1D (I)	−3.0	−12.5	82	72
1F (I)	−6.2	−11.6	81	68
	−2.8	−11.0	92	79
1F	0.2	−7.5	61	40
2A′	12.8	7.7	125	99
2B	−2.3	−11.8	80	69
2C	24.2	14.6	68	85
2D	−0.9	−11.9	63	66
2E	31.2	23.8	48	65
2G	−12.3	−22.7	91	72
2H	1.2	−12.0	87	88

[a] All velocities in km s^{-1}; radial velocities are heliocentric.

[b] Data marked by (I) were taken in 1981 November; all other data were taken during the 1982 November observing run.

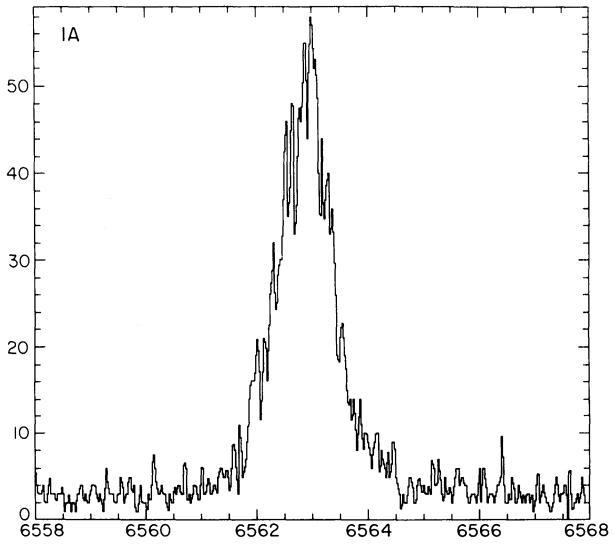

FIG. 2*a*

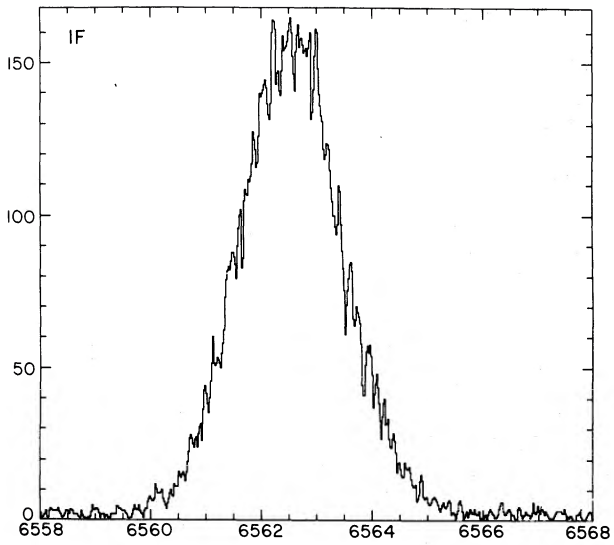

FIG. 2*b*

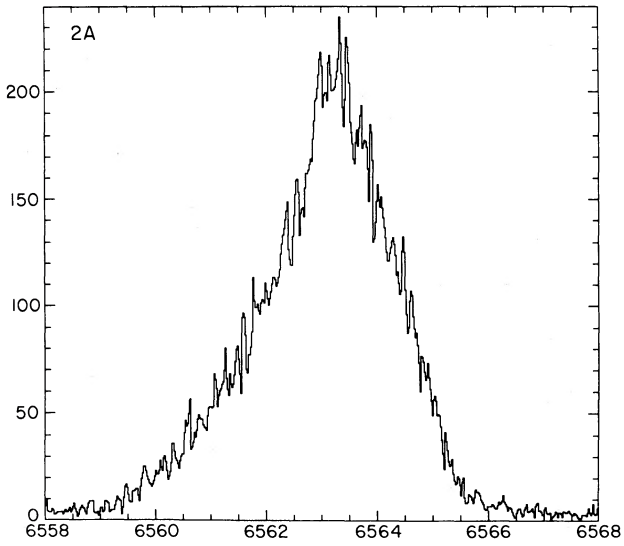

FIG. 2*c*

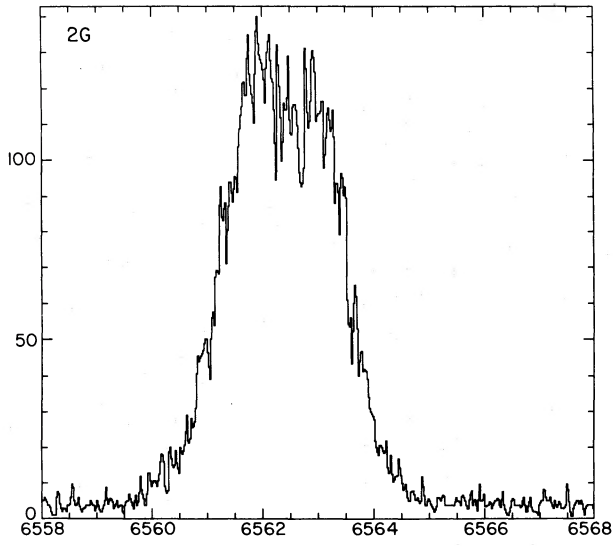

FIG. 2*d*

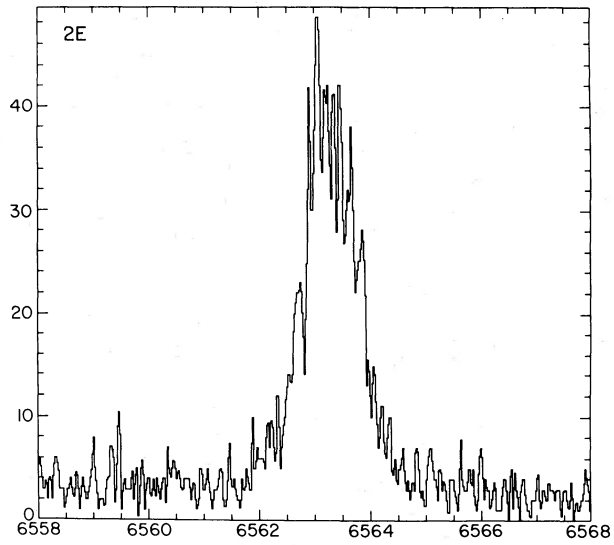

FIG. 2*e*

FIG. 2.—MMT echelle observations of Hα profiles of selected knots in HH 1 and HH 2. The vertical axis is counts per pixel: 1 pixel = 0.03 Å. (*a*) HH 1A; (*b*) HH 1F; (*c*) HH 2A′; (*d*) HH 2G; (*e*) HH 2E.

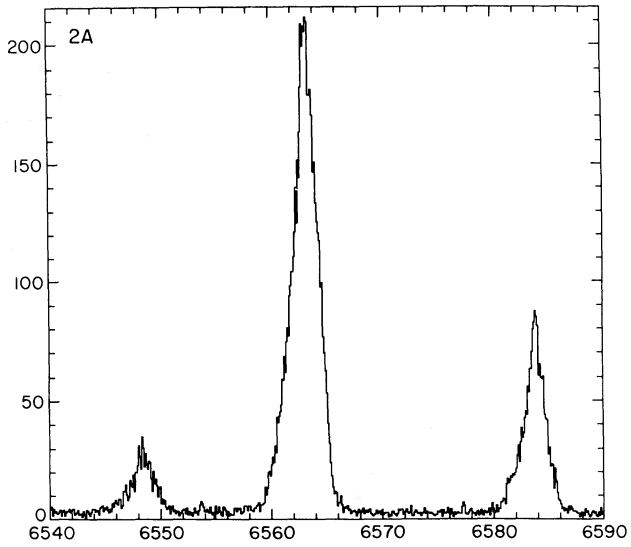

FIG. 3.—Spectrum of HH 2A′ showing the similarity in profiles of the Hα and [N II] lines

suggest that a large fraction of the shocked gas is being deflected through large angles to the original direction of motion.

b) Low-Resolution Spectra

The MMT spectrograph was used to measure emission line ratios at the same positions observed in high dispersion, using a 2″ aperture. The line fluxes relative to Hβ are listed in Table 2.

The results clearly indicate a variation in excitation across HH 1 from the changes in the O III/Hβ ratio. The knots in HH 2 also show a wide range of excitation; particularly note the low excitation knot HH 2E.

The ratio of [S II] $I(6717)/I(6730)$ is useful for its density sensitivity. Table 3 presents ratios which were obtained by simultaneously fitting two Gaussian profiles fixed at the doublet separation to the slightly blended lines. Densities were derived from computations by W. Blair (1982, private communication) which employed the transition probabilities of Mendoza and Zeippen (1982). The data indicate a variation in density of more than a factor of 2 over the relatively compact HH 1 object, while densities of the knots in HH 2 vary over an order of magnitude.

In Figure 5 we show the relationship between the FWHM of the Hα emission measured from the echelle data and the shock excitation, as defined by the O III/Hβ ratio. The

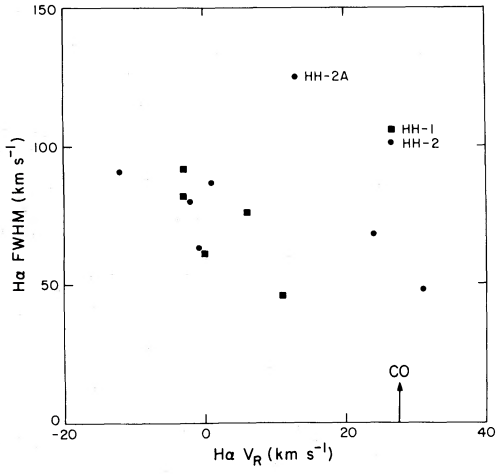

FIG. 4

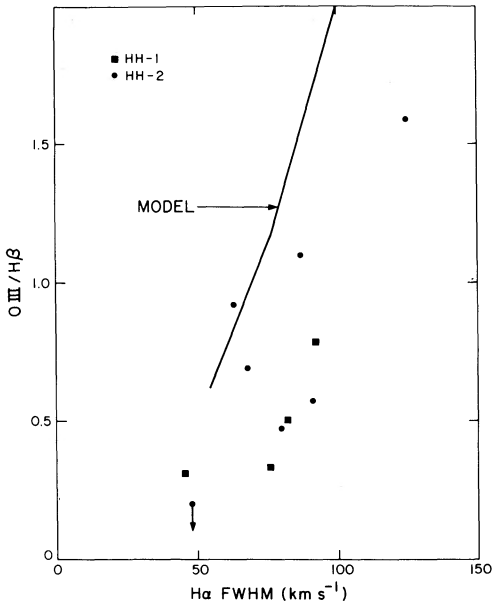

FIG. 5

FIG. 4.—The relationship between the radial velocity of the observed knots, as measured by the Hα emission centroid, and the FWHM of Hα.

FIG. 5.—The correlation between the [O III]/Hβ ratio and the Hα FWHM for the observed HH object knots. The relationship predicted by the bow shock model described in the text is also indicated.

TABLE 2

OBSERVED RELATIVE EMISSION LINE FLUXES

Identification	1A		1C	1D	1F	2A	2B	2C	2D	2E	2G	2H
Hγ λ3889	...	...	...	13	5	7	7	...	...	...	...	5
Ca II 3934	35	...	...	14	12	7	17	19	20	...	15	7
Ca II + He 3968	19	...	...	15	20	15	32	25	36	...	25	16
[S II] 4070	49	60	83	62	70	62	57	73	64	133	85	55
Hδ 4102	...	...	19	17	22	17	28	29	$\lesssim 20$	≤ 50	24	22
[Fe II] 4827	...	...	...	13	12	9	...	...	...	...	13	8
Hγ 4340	45	37	44	38	46	39	44	46	40	≤ 40	49	43
[Fe II] 4415	...	...	...	...	9	7	...	...	...	...	10	8
[Mg I] 4570	10	...	...	...	8	...	...	...	...	≤ 40	6	5
[Fe III] 4815	...	...	...	6	5	...	...	...	...	...	6	4
Hβ 4861	100	100	100	100	100	100	100	100	100	100	100	100
[O III] 4959	6	8	8	14	20	40	11	17	20	[a]	13	28
[O III] 5007	21	26	25	36	49	119	36	52	72	[a]	44	82
[Fe II] 5159	25	28	23	22	28	22	29	19	28	92	32	21
[N I] 5200	112	89	62	27	16	6	38	13	46	142	28	10
[Fe II] 5270	25	18	...	17	19	22	27	13	20	50	26	20
[Fe II] 5527	...	...	...	...	7	7	...	...	...	...	6	6
[N II] 5755	...	...	...	11	10	12	...	...	...	...	...	11
He I 5876	...	...	...	14	11	15	...	...	...	...	...	13
[O I] 6300	540	477	442	288	257	220	265	177	312	1200	288	232
[O I] 6364	175	165	146	93	87	72	88	50	102	417	88	69
[N II] 6548[b]	120	108	92	80	68	50	80	80	133	147	67	80
Hα 6563[b]	716	754	708	638	536	622	677	487	629	1240	511	566
[N II] 6583	362	323	275	239	203	151	239	240	398	440	201	239
[S II] 6724	805	774	571	295	249	129	383	435	770	2700	306	164
Estimated Hα flux[a] ...	1.2		1.2	0.8	3.6	4.3	0.5	0.3	0.3	0.3	0.8	2.5

[a] $5007 + 4959 \leq 20$.
[b] λ6548 assumed to be one-third of 6583, subtracted from Hα + [N II] blend.
[c] Flux in 2″ diameter circular aperture, in units of ergs cm^{-2} s^{-1}.

observations indicate that the line broadening is correlated with the shock velocity. In contrast, we note that Figure 6 shows a poor correlation between the O III/Hβ ratio and the transverse velocities inferred by Herbig and Jones (1981). The line width is thus a more accurate predictor of shock excitation than the proper motion. The reason for this result is probably that the proper motion measurements are affected by inhomogeneities in the ejecta or in the interstellar medium. New emission knots are known to appear on time scales as short as a year (Herbig 1969), and a superposition of such knots could yield an impression of motion unrelated to actual shock propagation.

TABLE 3

[S II] LINE RATIOS

Object	6717/6732	4070/6125	Ne (10^4 K)
1A[a]	0.707	0.0609	1300
	0.706	0.0775	1300
1C	0.723	0.145	1200
1D	0.598	0.210	2300
1F	0.572	0.281	2800
2A′	0.448	0.481	10^4
2B	0.794	0.149	880
2C	0.930	0.168	530
2D	0.693	0.0831	1400
2E	0.709	0.0493	1300
2G	0.444	0.278	10^4
2H	0.483	0.335	7000
H3	1.10	0.125	260

[a] Results for two separate exposures.

Although no attempt was made to perform absolute spectrophotometry of these HH objects, it is useful to indicate the approximate flux levels observed. The MMT spectrograph observations indicate that the Hα fluxes observed through the 2″ aperture ranged from ~0.3 to 4×10^{-13} ergs cm^{-2} s^{-1} (uncorrected for interstellar extinction), with HH 2A, 2H, and 1F being the brightest, and HH 2C, 2D, and 2E the faintest (cf. Table 2). These flux estimates are probably accurate to a factor of 2.

Plane-parallel single shock models predict a rapid change in the O III/Hβ ratio over a small range of shock velocity (Shull and McKee 1979). The moderate changes in O III/Hβ from knot to knot suggest that each cloud contains a range of shock velocities, a point which is incorporated into the model presented in the following section.

III. A MODEL FOR THE LINE EMISSION

a) Reddening

The first step in the analysis of these spectra is to make an estimate of the reddening. For HH 1, Brugel, Böhm, and Mannery (1981) obtain $E(B-V) = 0.47$ based on the [S II] $I(10320)/I(4070)$ ratio. Dopita (1978) obtained much higher reddening estimates, based on the [S II] $I(4070)/I(6720)$ ratio and his theoretical shock wave models, but a systematic calibration error was present in that data (Dopita, Binnette, and Schwartz 1982). We have computed some new shock models based on those of Raymond (1979) and Butler and Raymond (1980) with the new [S II] radiative transition probabilities of Mendoza and Zeippen (1982). These models predict a $I(4070)/I(6720)$ ratio 5%–10% lower for a given

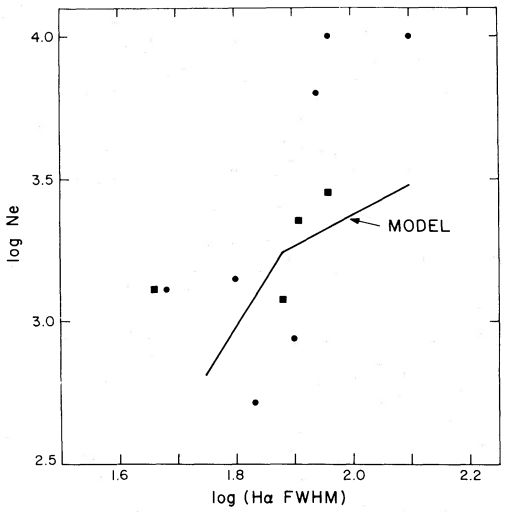

FIG. 6.—The relationship between the observed Hα FWHM and the electron density derived from the [S II] line ratio. Symbols are the same as in Fig. 5.

value of $I(6717)/I(6732)$ than shown in Figure 6 of Dopita (1978), leading to slightly lower values for the reddening.

We derived reddening values for objects with spectra of sufficient signal-to-noise ratios in the λ4070 emission. The results are $E(B-V) = 0.46, 0.17, 0.15, 0.11$, and 0.5 for HH 1A, 1A, 1F, 2A′, and 2G, respectively. Small negative values are derived for HH 2H and 2E. These values cannot be considered to be highly reliable due to uncertainties in the shock models, atomic parameters, reddening law, and calibration, but a similar variation in extinction would be inferred from the changes observed in the Balmer decrements. Some combination of these factors and the observational uncertainties must account for the apparently negative reddening which would be derived for HH 2C and HH 3; our estimates are that these negative reddening values are only $\sim 1.5\ \sigma$ results based on counting statistics alone.

In spite of the uncertainties, these results suggest that the reddening varies considerably from point to point within HH 1 and HH 2. This is not surprising in view of the great difference between the average reddening of HH 1 and the $E(B-V) = 1.7$ attributed to the CS star only 20″ away. The assumption of a single reddening value for HH 1 may be responsible for some of the difficulty in interpretation of the spectra. For instance, assuming $E(B-V) = 0.47$ for HH 1, Böhm-Vitense *et al.* (1982) found that I(O III λ1663) is twice the Hβ intensity, while Brugel, Böhm, and Mannery (1981) observed [O III] λ5007 to be one-third as strong as Hβ. Similarly, Brugel, Shull, and Seab (1982) observed λ1663 to be 2.5 times Hβ in HH 2H, while the optical [O III] lines were somewhat weaker than Hβ. The inferred ratios of UV to optical [O III] lines are an order of magnitude greater than predicted by shock models, and several times larger than the model independent upper limit given by the ratio of collision strengths.

If the reddening varies from $E(B-V) \sim 0.1$ to $E(B-V) > 0.4$ over HH 1, observations of the object as a whole will produce reddening estimates dependent on wavelength. Observations at short wavelengths will be very heavily weighted toward regions of low extinction. The hypothesis that the effective reddening is small for the UV observations eliminates the difficulties with luminosity and shape of the UV continuum (Ortolani and D'Odorico 1980; Böhm, Böhm-Vitense, and Brugel 1981; Böhm-Vitense *et al.* 1982). As proposed by Dopita, Binette, and Schwartz (1982) and confirmed for the case of HH 2H by Brugel, Shull, and Seab (1982), the continuum is probably hydrogen two-photon emission.

b) Relative Line Strengths

In view of the uncertainties and variations in the extinction, we cannot make useful comparisons between lines differing by more than a few hundred angstroms in wavelength. We can, however, learn a great deal from various pairs of nearby lines.

The ratio I([O III] λ5007)/I(Hβ) was used by Dopita (1978) and Raymond (1979) to infer shock velocities of ~ 80 km s^{-1}. The first *IUE* observations (Ortolani and D'Odorico 1980) showed that lines such as C IV λ1550 were far too strong to be produced in such a slow shock. The difficulty is due to the assumption of a single shock velocity. Table 2 clearly demonstrates variations in v_s among the knots, and it is highly probable that each knot contains a range of effective shock velocity. In particular, the bow shock model (Schwartz and Dopita 1978) predicts a range in effective shock velocity corresponding to the variation in obliquity of the shock.

c) Bow Shock Model

Whether HH objects are interstellar clouds in a stellar wind (Schwartz 1975), dense clumps of ejecta encountering interstellar gas (Norman and Silk 1979), or clumps in a stellar wind focused upon itself (Cantó 1980), the line emission is thought to arise from the combination of the bow shock in the low-density gas and the "cloudlet shock" in the higher density clump (Schwartz 1978).

An initial attempt to construct a bow shock model based on high-dispersion observations was made by Schwartz (1981). He showed that the velocity widths of several emission lines in HH 1 were roughly related to their excitation energies. This behavior was explained in terms of a model wherein a stellar wind shocks a dense interstellar cloudlet. The highest shock velocities are produced near the front edge of the cloud, where the shock is nearly normal; this region produces the high-excitation lines. The material flows away from a stagnation point after being shocked, producing a large velocity width in the line of sight (assumed to be roughly perpendicular to the flow direction given the small observed radial velocity). Far from the cloudlet, the shock is oblique, so the effective shock velocity is lower. Therefore lower excitation emission is preferentially formed in these regions. Since the flow diverges less, the low-excitation lines have narrower widths than the high-excitation emission.

We have constructed a quantitative model of a bow shock for comparison with the emission-line strengths and line profiles described above. It is assumed that the structure of the bow shock is the same as that computed by DeYoung and Axford (1967) for the shape of a cloud confined by the ram

pressure of its motion through a lower density medium. The lifetime of a cloud as an observable HH object is probably too short to establish this shape, but it is likely that the cloud would achieve the correct shape either during its passage outward from the central star (for the interstellar bullet model) or by spending sufficient time immersed in a lower density wind (in Schwartz's model). We also make the assumption that the shock is radiative. When the gas cools to $\sim 10^4$ K it is compressed by a factor of ~ 60 for the parameters we will consider; because of this large compression, the shape of the bow shock will closely follow the shape of the cloudlet. Typical cooling distances for such shocks are $\sim 10^{14}$ cm, compared with observed knot sizes of $\sim 10^{16}$ cm.

The emission-line intensities and line profiles can then be computed. The angle between the normal to the bow shock and the preshock flow direction, θ, is given by the DeYoung and Axford (1967) model. The normal component, $v_{\max} \cos \theta$, is the effective shock velocity, and each particle entering the shock is assumed to emit as though it were passing through a steady-flow plane-parallel normal shock of $v_s = v_{\max} \cos \theta$. We then make discrete increments in intervals of 0.1 in $\cos \theta$ and calculate the relative area of the bow shock from the DeYoung and Axford shape. We weight the emission from each $\cos \theta$ interval by the number of Hβ photons per hydrogen atom passing through a $v_{\max} \cos \theta$ shock and average the line strengths relative to Hβ. While this could be done with existing tables of shock models (Raymond 1979; Shull and McKee 1979), we have computed a grid of models with a preshock density of 100 cm^{-3} to match the densities inferred from the [S II] line ratio, and we have extended the models to higher shock velocities. The charge transfer coefficients used by Butler and Raymond (1980) were used, along with corrections to several excitation rates mentioned by Raymond *et al.* (1981), the [S II] A values given by Mendoza and Zeippen (1982), and collision strengths from Pradhan (1978). The "cosmic" abundance set of Allen (1973) was used.

There are several major sources of uncertainty in the models. The DeYoung and Axford shape may not be a reasonable approximation, given the complexity of the flow; however, the general results are not very sensitive to the details of the shape. Second, the preshock ionization fraction for each value of $v_{\max} \cos \theta$ was taken to be the self-consistent value determined by the ionizing flux emitted by a shock of that velocity. Preshock ionization fractions were in approximate agreement with those given by Shull and McKee (1979). Though this is a reasonable assumption for a first attempt, the mean free path of an ionizing photon in the preshock gas is only 5 or 10 times smaller than the cloud size. Thus photons produced in the nearly normal incidence region at the tip of the bow shock will preionize gas ahead of the more oblique part of the flow to some extent. Third, plane-parallel models have been used to approximate the emission from a complex flow pattern: The total energy emitted and the postshock temperature should be correct, so UV lines, [O III] lines, and Balmer lines predicted by the model are likely to be reliable, but forbidden lines formed at lower temperatures are likely to be affected by details of the post-shock flow pattern. Thus while the model provides a reasonable guess at the average emission from such a bow shock, it is not precise enough for a detailed fit to observations.

d) Predictions of Bow Shock Model

Table 4 lists emission-line strengths relative to Hβ = 100 for 160, 200, and 300 km s^{-1} bow shock models. These values are comparable to the transverse velocities inferred by Herbig and Jones (1981) for HH 1 and HH 2, although shock velocities of at least 300 km s^{-1} are required if X-rays are to be emitted (Pravdo and Marshall 1981). The weighting of effective shock velocities is such that Balmer lines are mostly produced by $v \cos \theta = 70$–110 km s^{-1} oblique shocks, while [O III] and the UV lines are largely produced in the $v \cos \theta \geq 100$ km s^{-1} region. The [S II] lines should reflect a weighted average of the compression at $\sim 10^4$ K, ranging from ~ 200 at the stagnation point to ~ 10 near the periphery. These particular models give $I(6717)/I(6732) = 0.56$ to 0.88, but this prediction can be greatly affected by details of the flow geometry.

Comparison of Table 4 with the MMT spectra shows reasonable overall agreement, except for the low-excitation lines, which are predicted to be much weaker than observed. In this regard, HH 2E shows strongly enhanced low-excitation emission. This may be connected with the peculiar proper motion of this object; the measurements of Herbig and Jones (1981) indicate very small motion for HH 2E in a much different orientation than for the other knots. The strengths of the UV lines relative to each other are similar to those observed by Böhm, Böhm-Vitense, and Brugel (1981) for HH 1 as a whole and by Brugel, Shull, and Seab (1982) for HH 2H. The strengths of the UV lines relative to Hβ given by those authors are somewhat greater than predicted, but if the effective reddening in the UV is smaller than that used by Böhm, Böhm-Vitense, and Brugel (1981) (as suggested in the previous section) the agreement is quite good.

We can also predict the line widths on the basis of this model. When gas enters an oblique shock, three-fourths of the normal component, $v \cos \theta$, is thermalized. As the gas cools

TABLE 4

BOW SHOCK MODELS: LINE INTENSITIES RELATIVE TO Hβ, Hα WIDTH, AND [S II] INTENSITY RATIO

SPECIES	$v_{\max}$ 160 km s^{-1}	200 km s^{-1}	300 km s^{-1}
N V λ1240	8	36	125
C II λ1335	4	13	7
O IV + Si IV λ1400	20	38	103
C IV λ1550	76	226	370
He II λ1640	6	22	48
O III] λ1662	22	43	112
C III] λ1909	81	117	249
[O II] λ3727	123	220	245
[S II] λ4070	8	10	28
Hβ	100	100	100
[O III] λ5007 + λ4959	64	117	286
[N I] λ5200	3	6	13
[O I] λ6300 + λ6363	86	96	237
[N II] λ6548 + λ6584	83	97	196
Hα	330	317	301
[S II] λ6717 + λ6732	44	46	80
Hα FWHM	56 km s^{-1}	76 km s^{-1}	126 km s^{-1}
$I(6717)/I(6732)$	0.88	0.66	0.56

and undergoes compression, the remaining one-fourth $v \cos \theta$ decreases to zero. Thus for lines formed at $\sim 10^4$ K, the postshock gas velocity is just the tangential component of the preshock velocity, $v \sin \theta$. The gas flows along parallel to the shock, and its component normal to the cloud axis is $v \sin \theta \cos \theta$. Performing the same average as adopted for the emission-line strengths, we find an average normal component of $0.35 v_{\max}$. Assuming that our line of sight is perpendicular to the cloudlet axis (since transverse motions of 200–300 km s^{-1} are reported by Herbig and Jones 1981, while our Doppler shifts show $\lesssim 30$ km s^{-1}), we average over azimuth and identify $0.17 v_{\max}$ as roughly the HWHM expected for the lines, and FWHM $\approx 0.35 v_{\max}$. Thus the bow shock model for $v_{\max} = 200$ km s^{-1} predicts ~ 70 km s^{-1} line widths, in agreement with the HH 1 C, D, and F profiles.

It is necessary to consider the contribution of thermal broadening to the line widths in addition to the macroscopic motions. This is complicated by the composite nature of the Hα line. Some of the Hα emission is produced by recombination at $\sim 10^4$ K, but a substantial fraction (55%, 53%, and 27% for the 160, 200, and 300 km s^{-1} models, respectively) comes from collisional excitation of neutral hydrogen entering the shock at temperatures typically $\sim 10^5$ K. We have combined the thermal broadening quadratically with the flow velocities in arriving at our estimated line widths.

The most definite predictions of the model are (1) that O III/Hβ should be quite small for $v_{\max} \lesssim 150$ km s^{-1} and should be correlated with $v_{\max}$, and (2) that the FWHM of the emission lines should be 0.3–$0.4 v_{\max}$ plus any thermal or turbulent width. The line widths have been calculated on the assumption that the motion is essentially transverse to the line of sight. In the case of shocks propagating more nearly in the line of sight, as for example in HH 32 (Mundt, Stocke, and Stockman 1983), the model predicts that emission should be spread in radial velocity from 0 to $v_{\max}$, with the maximum of emission peaking at $\sim \frac{1}{3}$–$\frac{1}{2} v_{\max}$.

The predicted relationship between the O III/Hβ ratio and the Hα FWHM is shown in Figure 5. The model agrees with the general trend or slope of the observed correlation. However, the predictions result in either too small an O III/Hβ ratio for a given line width, or line broadening that is too small for a given shock excitation. The discrepancy may indicate that other broadening mechanisms have been neglected, as detailed below, or that there are departures from the assumed bow shock shape.

As shown in Figure 6, the model predicts a correlation between the shock velocity and the electron density for an assumed constant initial preshock density. The prediction is in qualitative agreement with the observations, but the data clearly indicate a much more rapid increase of electron density with increasing shock velocity. Note that there is no reason to suppose all objects have the same preshock density.

d) Further Discussion of Bow Shock Model

If ions and electrons equilibrate only through Coulomb collisions, the fraction of Hα produced collisionally will be greatly enhanced, and it will reflect a higher kinetic temperature (Ohtani 1980) compared with our assumption of instant electron-ion equilibration by plasma turbulence. This would increase the predicted Hα widths by ~ 10 km s^{-1}. In addition, Hα emission produced just behind the shock will still have a significant portion of the normal component $v \cos \theta$. This could increase the Hα width by another 10 km s^{-1}.

In order to check our estimates of thermal and turbulent velocities, we may attempt to separate the thermal and turbulent contributions to the line widths. For instance, Shull *et al.* (1982) found temperatures of $\sim 20{,}000$ K and turbulent velocities of ~ 30 km s^{-1} from Hα and [N II] profiles of the Cygnus Loop. If we assume that the nonthermal part of the velocity width has a Gaussian profile and make the assumption that Hα and [N II] lines are formed in the same region, we can use the usual methods (e.g., Shull *et al.* 1982) to derive the temperature. This procedure yields kinetic temperatures of $\sim 10^5$ K for the knots in HH 1, in agreement with the models if electron-ion equilibration is assumed to be slow. However, four of the seven knots in HH 2 would require very small (or even negative) temperatures, and two of the others would require unreasonably high temperatures. Some of the line profiles are obviously non-Gaussian, but most of the difficulty is probably due to the assumption that Hα and N II are formed in the same region. We are therefore unable to directly assess the contribution of collisional excitation of neutrals entering the shock to the Hα intensity.

While the model is not precise enough for a detailed comparison with the line intensities, several general features should be noted. The strengths of the carbon lines relative to those of oxygen suggest that carbon is somewhat depleted, as would be expected for a shock in a dense interstellar cloud. This might not be expected in the focused wind model (Cantó 1980). The He II λ1640 line was calculated with the assumption of case A; all He II Lyβ photons (λ256) either escape or cause photoionization. However, the optical depth for resonant scattering of λ256 photons is not negligible, and such a scattering can convert a λ256 photon to a λ304 and a λ1640 photon. Thus the model prediction for $I(1640)$ is likely to be an underestimate. The predicted intensity of C II λ1335 is much lower than observed, possibly because the contribution of low-velocity shocks has been underestimated. The absence of detected N V emission suggests that $v_{\max}$ is no larger than 300 km s^{-1}.

The most noteworthy feature of the optical spectrum is the [O III]/Hβ ratio. With the inclusion of charge transfer (cf. Butler and Raymond 1980) and the assumption that preshock gas is ionized only by the EUV emission of the shock, plane-parallel models show a very sudden jump in [O III]/Hβ from 0.02 at $v_s = 100$ km s^{-1} to 5.4 at $v_s = 120$ km s^{-1}. Plane-parallel, steady flow shocks could produce the [O III] to Hβ ratios seen in most of the knots only if $v_s = 110 \pm 5$ km s^{-1} in nearly all knots or if the preshock gas were ionized. Thus the observed [O III]/Hβ ratios in themselves provide fairly strong evidence that each knot contains a range of shock velocities. The range of shock velocities explains naturally the observations of UV emission lines which would not be produced in a single shock slow enough to produce the [O III]/Hβ ratio (Ortolani and D'Odorico 1980; Böhm, Böhm-Vitense, and Brugel 1981). Nonsteady plasma shocks can produce some of the characteristics of the observed spectra (Dopita, Binette, and Schwartz 1982). Such shocks appear to be most promising as an explanation for the very low excitation knots. However, we note that HH 1A and HH 2E, whose spectra closely resemble the low-excitation objects modeled by Dopita, Binnette, and Schwartz (1982),

have line widths far too large to be produced by the 35 km s^{-1} shock of the nonsteady model.

The strengths of the lowest excitation lines are underestimated by the bow shock models. The emission in these lines is probably the most uncertain prediction, even in the context of simple plane-parallel shocks. The shape assumed for the bow shock may underestimate the contribution of the low effective shock velocity regions near the periphery.

Besides the consideration of other bow shock geometries, there are two major modifications to the model which seem likely to be necessary. The first is inclusion of emission from the clouds. If a cloud has only recently encountered high-density gas, a low-velocity cloud shock might contribute to the Balmer lines and low excitation forbidden lines (see Schwartz 1975). If the density contrast is greater than 100, this shock may produce mostly molecular emission, but if the contrast is smaller the cloud shock would contribute substantially to the Balmer lines, [O I], [N I], and [S II] emission. The second interesting possibility is mixing of cloud material with gas which has passed through the bow shock. The flow along the surface of the cloud is likely to be Kelvin-Helmholtz unstable. Mixing of cloud gas into the postshock flow implies a reduction of velocity to conserve momentum. If the mixing occurs on a small enough scale, neutral hydrogen could be mixed into the postshock cooling zone. This would enhance Balmer line excitation and increase the Hα/Hβ ratio. It could drastically reduce the emission of [O II], [N II], and [O III] without affecting the UV lines. Charge transfer would then enhance the [O I] and [N I] emission.

IV. IMPLICATIONS FOR MODELS OF HH OBJECTS

a) *Nature of HH Objects*

Herbig and Jones (1981) showed that the knots in HH 1 and HH 2 have large proper motions aligned in directions nearly opposite the Cohen-Schwartz star. Because of this alignment, and because the CS star is the only known infrared source nearby (Cohen and Schwartz 1979), it seems very likely that HH 1 and HH 2 are excited in some fashion by this heavily extincted T Tauri star. We now consider the implications of our observations for the nature of the pre–main-sequence stellar activity which produces HH objects.

Schwartz (1975) initially suggested that HH objects were stationary condensations in the surrounding interstellar medium which are shocked by a stellar wind. This picture was modified to allow the wind to accelerate the condensation or cloud to high velocities, in view of the observed radial velocities or proper motions (Schwartz 1978; Schwartz and Dopita 1980). Hereafter we shall refer to this picture as the SD model.

An opposing picture, in which HH objects are dense clouds plowing into lower density interstellar medium, was proposed by Norman and Silk (1979) and by Rodríguez *et al.* (1980). This scenario has been called the "interstellar bullet" model. The HH objects could be the remnants of a dense cocoon initially surrounding the pre–main-sequence star, which is broken up and accelerated by the stellar wind (Kahn 1974; Dopita 1974).

It is not easy to distinguish between the two models on the basis of present knowledge. Prior to this study, the most significant test was provided by the astrometric study of Herbig and Jones (1981). They noted that new emission knots are moving quite rapidly a few years after their appearance. This is a severe problem for the SD picture, because the acceleration of the cloud is expected to take hundreds of years. We also note that HH object knots have been observed to appear suddenly, on time scales as short as a year. It it easy to explain this behavior if the objects are supposed to be dense clouds plowing into an inhomogeneous medium. The SD picture requires a large variation of the impacting stellar wind in either space or time.

Our observations provide two results in favor of the bullet model. First, we have shown that the maximum shock velocity in our bow shock model, v_{max}, is more like 200 km s^{-1} than than 100 km s^{-1}. The proper motions also indicate tangential velocities $\sim$200 km s^{-1}. The simplest explanation of this result is that the shock is propagating ahead of a dense cloudlet into lower density interstellar medium, in which case $v_{max} \sim v$(tangential). Otherwise, one must suppose that the stellar wind coincidentally has a velocity twice the velocity of the shocked cloud. In addition, we note that observations of T Tauri stars generally indicate wind velocities more commonly $\sim$100–200 km s^{-1} than 400 km s^{-1} (cf. Hartmann 1982 and references therein).

The second piece of evidence in favor of the bullet model is the relationship of shock velocities to the observed proper motions. If HH objects are dense knots plunging into a less dense, stationary interstellar medium, v_{max} should be proportional to the observed proper motion. The opposite correlation is predicted by the SD model, in which the shock velocity is given by the difference between the stellar wind velocity and the cloudlet velocity.

Assuming similar geometries for the knots, our bow shock model predicts that v_{max} can be inferred from either the shock excitation, as indicated by the O III/Hβ ratio, or by the line widths, which should be proportional to v_{max}. In Figure 7 we show the relationship between the proper motions of the knots in HH 1 and HH 2, and the O III/Hβ ratio. No correlation is observed in this diagram, favoring neither model. Figure 8 exhibits the relation between the velocity

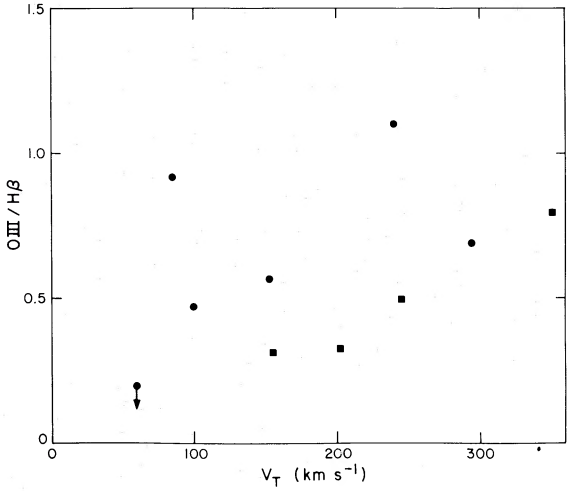

FIG. 7.—Plot of the [O III]/Hβ ratio in several HH object knots vs. the tangential velocities inferred from proper motions. Symbols are the same as in Fig. 5.

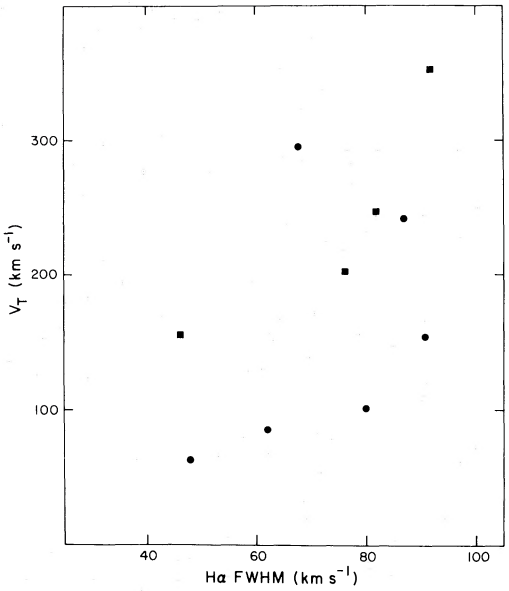

FIG. 8.—Plot of the inferred tangential velocities vs. the Hα FWHM. Symbols are the same as in Fig. 5.

width of Hα and the proper motion. Here we observe a correlation in the sense predicted by the bullet model. This correlation is marginal; the correlation coefficient is only 0.54, which indicates a result significant only at the 90% level. However, in addition to this result, we note that the knots of HH 1 considered alone indicate positive correlations independently in both diagrams. The knots in HH 1 are more compactly distributed and have proper motions much more closely aligned with the CS star than the knots in HH 2, so that it is plausible that correlations are easier to observe in the former object.

One difficulty with the bullet model is that the proper motion vectors exhibit a dispersion so large that it is difficult to see how the knots keep together during the time of flight from the star. Herbig and Jones (1981) suggest that these objects are regions "across which transient bright knots move rapidly, appearing on the side toward the CS star and fading before they have moved beyond the far boundary." We propose that the site for the overall HH object emission is a region of increased density in the gas surrounding the CS star, and that inhomogeneity of this medium into which the dense knots move causes the deviation from motion directly opposite the CS star.

Mundt, Stocke, and Stockman (1983) suggested that their observations of HH 32 favor the SD model. Their argument depends upon the absence of [N II] emission from HH 32B, which has a high (260 km s^{-1}) radial velocity. The shock velocity must be low (<70 km s^{-1}) to avoid producing [N II]. This is impossible to achieve in a bullet bow shock model, but easy in the SD picture, where the shock velocity is the difference of the wind and cloudlet velocities. However, it is also possible to produce a slow shock in the bullet model if the emission comes from a cloudlet shock (cf. Schwartz and Dopita 1978). In this case we would expect that the Hα emission width would be narrow; this is compatible with the observations of Mundt, Stocke, and Stockman (1983). A cloudlet shock interpretation would also be required by the small line widths and the absence of [O III] in HH 47A and HH 47C (Dopita, Schwartz, and Evans 1982).

At present, we tentatively conclude that the evidence favors the bullet model over the SD picture. It may not be possible to construct a single, simple model for the emission of HH objects. In any given object, one may observe cloudlet shocks as well as bow shocks, and bullets may shock with more dense interstellar medium. The bullet model is clearly an idealization of what must be a very complicated situation. Other HH objects should be observed with high resolution in order to test the reality of these correlations.

b) Origin of HH Objects

It seems clear that HH objects must be accelerated in some fashion by the wind from a pre–main-sequence star. However, it has proved difficult to make this connection plausible in a quantitative fashion. Models in which HH objects are excited by an isotropic stellar wind seem to imply mass loss rates $\dot{M} \geq 10^{-5}\ M_\odot\ \mathrm{yr}^{-1}$ (Schwartz and Dopita 1978; Mundt and Hartmann 1983), while studies of mass loss from T Tauri stars suggest winds with $\dot{M} \sim 10^{-8}\ M_\odot\ \mathrm{yr}^{-1}$ (deCampli 1981; Hartmann, Edwards, and Avrett 1982). This discrepancy, coupled with the asymmetric, "bipolar" appearance of the outflows, has led to the development of models in which an initially isotropic wind is channeled or focused by the ambient interstellar medium into two opposing, locally dense flows (Cantó 1980; Cantó and Rodríguez 1980; Königl 1982). In these models, the gas cloud surrounding the pre–main-sequence star is presumed to have collapsed into a flattened arrangement, with the density gradient in the direction of the angular momentum vector and/or ambient magnetic field. The flow is then preferentially directed perpendicular to the plane of the flattened cloud.

In the model developed by Cantó (1980) and Cantó and Rodríguez (1980), the stellar wind develops ovoidal cavities in the surrounding medium. The wind shocks, cools, and then slides along the surfaces of the cavity, conserving momentum in the direction parallel to the wall. This shocked wind is then brought together or focused at the far ends of the cavities. Although it was originally supposed that HH objects result from the focused material shocking with itself, the proper motion and radial velocity data make it more likely that the objects are clouds broken off from the walls of the cavity and accelerated in the general flow. This mechanism is attractive, in that Cantó and Rodríguez suggest that the mass loss requirements might be reduced to a few times $10^{-7}\ M_\odot\ \mathrm{yr}^{-1}$ in this way. However, it is difficult to evaluate the efficiency of this model. In particular, it is not clear whether small inhomogeneities in the cavity wall would not disrupt the sliding flow, reducing the efficiency of the mechanism considerably.

An alternative picture was presented by Königl (1982), who supposed that a pressure-driven bubble might be driven into the surrounding medium if the shocked stellar wind cannot cool quickly by radiation. Königl suggested that the expansion of the bubble into an anisotropic medium might produce nozzles in the cold gas, which accelerate the shocked wind to supersonic velocities. This picture has the advantage of avoiding the problem of irregularities in the cavity wall. The principal difficulty with accepting this model is that the

velocity of the outflowing material in the supersonically accelerated jets is presumably controled by the detailed geometry of the nozzle. If the ambient medium is inhomogeneous, as seems likely, it is not immediately apparent why the opposing nozzles accelerating HH 1 and HH 2 should have produced similar overall ejection velocities.

In the previous section we showed that the observations favor the description of HH objects as dense cloudlets shocking with less dense interstellar medium. Such cloudlets might be produced by the breakup of a "cocoon" surrounding a newly formed star under the impact of a stellar wind (Norman and Silk 1979; Rodríguez *et al.* 1980; Kahn 1974; Dopita 1974; Chevalier 1983). We can make an estimate of the mass loss rates required by this picture if we can first estimate cloudlet masses. As mentioned earlier, the absolute fluxes observed are roughly consistent with the models if it is assumed that the emitting knots approximately fill the 2″ aperture. Photographs also suggest knot sizes ~1″–2″ (Herbig and Jones 1981). Therefore we shall assume that the typical knot or cloudlet is resolved and is of ~2″ in size. We can then estimate the cloudlet mass in two ways, assuming a lifetime ~30 years, based on the observed variability of many knots (Herbig 1969). First, we require the cloudlets to have sufficient momentum that they do not appreciably slow down in their lifetimes (Herbig and Jones 1981) upon shocking with ambient material with $N \sim 10^2$ cm^{-3}. Second, we can use estimates of (typical) cloudlet luminosities ~0.1–1 $L_\odot$ (Böhm, Böhm-Vitense, and Brugel 1981; Böhm-Vitense *et al.* 1982). If we equate the cloudlet luminosity to the initial kinetic energy of the cloudlet divided by the lifetime, and let $v_c \sim 200$ km s^{-1}, the cloudlet mass can be estimated. Using either the momentum or energy argument, we find cloudlet masses $\gtrsim 10^{-6}\ M_\odot$.

Then from conservation of momentum, we estimate

$$\dot{M} v t \left(\frac{\Omega}{4\pi}\right) \gtrsim M_c v_c ,$$

where v is the wind velocity and Ω is the solid angle the cloudlet subtends at the star. We assume $v \sim v_c$, Ω = constant, cloudlets ~ 2″ ~ 10^{16} cm in size, and $M_c \sim 10^{-6}\ M_\odot$. The travel time from the CS star to HH 1 at 200 km s^{-1} is ~250 yr; to HH 2, the time is ~10^3 yr. Inserting these values results in mass loss rates $\gtrsim 10^{-5}\ M_\odot$ yr^{-1} (see also Mundt and Hartmann 1983).

Now consider the stellar wind problem. Hartmann, Edwards, and Avrett (1982) calculated wind models for T Tauri stars with $L \sim 2\ L_\odot$ and were able to match observations with mass loss rates $\sim 10^{-8}\ M_\odot$ yr^{-1}. Cohen and Schwartz (1979) estimate that the luminosity of the star is $>10\ L_\odot$. The upper limit to the luminosity is uncertain because the far infrared flux is unknown, but it may well be as large as 30 $L_\odot$ (Mundt and Hartmann 1983). In this case the mass loss rates of Hartmann, Edwards, and Avrett (1982) might be scaled up by roughly the increase in the adopted stellar luminosity, so that it might be possible to reconcile mass loss rates as high as $10^{-7}\ M_\odot$ yr^{-1} with the theory (see also DeCampli 1981). However, this is still much smaller than the mass loss rates required by the HH objects in the absence of focusing. Even if we let $\frac{1}{2}\dot{M}v^2 = L = 30\ L_\odot$, $\dot{M} \sim 5 \times 10^{-6}\ M_\odot$ yr^{-1}. This is certainly an extreme upper limit.

Although focusing may play an important role in ejecting HH objects, particularly in terms of producing bipolar flow, we suspect that there may be a problem with assuming Ω = constant. A dense cloud with $T \sim 300$ K will have a sound speed ~1 km s^{-1}, so that the sound travel time across a cloudlet of 10^{16} cm is ~3×10^3 yr. Thus it is questionable whether knots in HH 1 and HH 2 have really expanded substantially in the last several hundred years. Furthermore, even if the cloudlets are in pressure equilibrium, it is not obvious that Ω = constant. Elmegreen and Morris (1979) calculated that clouds confined by the ram pressure of a stellar wind (in a different context) should vary in size as r^n, where r is the radial distance and $n \lesssim \frac{2}{3}$.

The net result of these considerations is to suggest that the cloudlets subtended a much larger angle as seen from the CS star when ejected than at present. This effect could reduce the mass loss rate requirements considerably even in the absence of any focusing. Although this picture is speculative at present, it may be possible to perform hydrodynamic calculations to test this hypothesis.

V. CONCLUSIONS

We have presented high spectral and spatial resolution observations of line emission in HH 1 and HH 2, showing that the structure can vary considerably over scales of 2″ or less. The Hα and [N II] lines are very broad in some of the knots indicating mass motions in the line of sight with a total velocity width of up to 300 km s^{-1}. These widths are correlated with the excitation of the emission line spectra of the knots. The Hα line widths and UV spectra can be reconciled in terms of a bow shock model, with a maximum shock velocity ~200 km s^{-1}. This revision of shock velocities from previous models indicating $v_s \sim 100$ km s^{-1} matches the transverse velocities ~200–300 km s^{-1} inferred from proper motion studies. The simplest explanation of this agreement of the two velocities is that HH objects are dense clouds running into a less dense medium. Correlations of the emission properties of the knots indicate marginal support for the bullet model.

It is difficult to reconcile the energy requirements for HH objects with normal T Tauri star winds. Focusing mechanisms may alleviate this difficulty. One possibility for further investigation is that if HH objects start off close to the exciting star, they may have subtended a larger solid angle than at present, and hence may have been accelerated by a much larger fraction of the (isotropic) stellar wind.

We wish to acknowledge the assistance of the MMTO staff in obtaining these observations, and to thank Neal Burnham for his help in reducing the data. This work was supported in part by NASA grant NAGW-100.

REFERENCES

Allen, C. W. 1973, *Astrophysical Quantities* (3d ed; London: Athlone Press).
Böhm, K.-H., Böhm-Vitense, E., and Brugel, E. W. 1981, *Ap. J.* (*Letters*), **245**, L113.
Böhm-Vitense, E., Böhm, K. H., Cardelli, J. A., and Nemec, J. M. 1982, *Ap. J.*, **262**, 224.
Brugel, E. W., Böhm, K.-H., and Mannery, E. 1981, *Ap. J. Suppl.*, **47**, 117.
Brugel, E. W., Shull, J. M., and Seab, C. G. 1982, *Ap. J.* (*Letters*), **262**, L35.
Butler, S. E., and Raymond, J. C. 1980, *Ap. J.*, **240**, 680.
Cantó, J. 1980, *Astr. Ap.*, **86**, 327.
Cantó, J., and Rodríguez, L. F. 1980, *Ap. J.*, **239**, 982.

Chevalier, R. 1983, *Ap. J.*, **268**, 753.
Cohen, M., and Schwartz, R. D. 1979, *Ap. J.* (*Letters*), **233**, L77.
DeCampli, W. 1981, *Ap. J.*, **244**, 124.
DeYoung, D. S., and Axford, W. I. 1967, *Nature*, **216**, 129.
Dopita, M. A. 1974, *Nature*, **250**, 397.
———. 1978, *Ap. J. Suppl.*, **37**, 117.
Dopita, M. A., Binette, L., and Schwartz, R. D. 1982, *Ap. J.*, **161**, 183.
Dopita, M. A., Schwartz, R. D., and Evans, I. 1982, *Ap. J.* (*Letters*), **263**, L73.
Elmegreen, B. G., and Morris, M. 1979, *Ap. J.*, **229**, 593.
Hartmann, L. 1982, *Ap. J.* (*Suppl.*), **48**, 109.
Hartmann, L., Edwards, S., and Avrett, E. H. 1982, *Ap. J.*, **261**, 279.
Herbig, G. H. 1969, in *Non-Periodic Phenomena in Variable Stars*, ed. L. Detre (Budapest: Academic Press), p. 75.
Herbig, G. H., and Jones, B. F. 1981, *A.J.*, **86**, 1232.
Kahn, F. D. 1974, *Astr. Ap.*, **37**, 149.
Königl, A. 1982, *Ap. J.*, **261**, 115.
Latham, D. 1982, in *IAU Colloquium 67, Instrumentation for Astronomy with Large Optical Telescopes*, ed. C. M. Humphries (Dordrecht: Reidel), p. 259.
Loren, R. B., Evans, N. J., and Knapp, G. R. 1979, *Ap. J.*, **234**, 932.
Mendoza, C., and Zeippen, C. J. 1982, *M.N.R.A.S.*, **199**, 1025.
Mundt, R., and Hartmann, L. 1983, *Ap. J.*, **268**, 766.
Mundt, R., Stocke, J., and Stockman, H. S. 1983, *Ap. J.* (*Letters*), **265**, L71.
Norman, C., and Silk, J. 1979, *Ap. J.*, **228**, 197.
Ohtani, W. 1980, *Pub. Astr. Soc. Japan*, **32**, 11.
Ortolani, S., and D'Odorico, S. 1980, *Astr. Ap.*, **83**, 68.
Pravdo, S. H., and Marshall, F. E. 1981, *Ap. J.*, **248**, 591.
Raymond, J. C. 1979, *Ap. J. Suppl.*, **39**, 1.
Raymond, J. C., Black, M. W., Dupree, A. K., Hartmann, L., and Wolff, R. S. 1981, *Ap. J.*, **246**, 100.
Rodríguez, L. F., Moran, J. M., Ho, P. T. P., and Gottlieb, E. W. 1980, *Ap. J.*, **235**, 845.
Schwartz, R. D. 1975, *Ap. J.*, **195**, 631.
———. 1978, *Ap. J.*, **228**, 884.
———. 1981, *Ap. J.*, **243**, 197.
Schwartz, R. D., and Dopita, M. A. 1980, *Ap. J.*, **236**, 543.
Shull, J. M., and McKee, C. F. 1979, *Ap. J.*, **227**, 131.
Shull, P., Jr., Parker, R. A. R., Gull, T. R., and Dufour, R. J. 1982, *Ap. J.*, **253**, 682.

L. HARTMANN and J. C. RAYMOND: Center for Astrophysics, 60 Garden Street, Cambridge, MA 02138